JACS
JOURNAL OF THE AMERICAN CHEMICAL SOCIETY
Article
pubs.acs.org/JACS

Key Roles of Lewis Acid–Base Pairs on $Zn_xZr_yO_z$ in Direct Ethanol/Acetone to Isobutene Conversion

Junming Sun,[†] Rebecca A. L. Baylon,[†] Changjun Liu,[†] Donghai Mei,[‡] Kevin J. Martin,[§] Padmesh Venkitasubramanian,[§] and Yong Wang*[,†,‡]

[†]The Gene & Linda Voiland School of Chemical Engineering and Bioengineering, Washington State University, Pullman, Washington 99164, United States

[‡]Institute for Integrated Catalysis, Pacific Northwest National Laboratory, Richland, Washington 99352, United States

[§]Archer Daniels Midland Company, 1001 N Brush College Road, Decatur, Illinois 62521, United States

Supporting Information

ABSTRACT: The effects of surface acidity on the cascade ethanol-to-isobutene conversion were studied using $Zn_xZr_yO_z$ catalysts. The ethanol-to-isobutene reaction was found to be limited by the secondary reaction of the key intermediate, acetone, namely the acetone-to-isobutene reaction. Although the catalysts with coexisting Brønsted acidity could catalyze the rate-limiting acetone-to-isobutene reaction, the presence of Brønsted acidity is also detrimental. First, secondary isobutene isomerization is favored, producing a mixture of butene isomers. Second, undesired polymerization and coke formation prevail, leading to rapid catalyst deactivation. Most importantly, both steady-state and kinetic reaction studies as well as FTIR analysis of adsorbed acetone-d_6 and D_2O unambiguously showed that a highly active and selective nature of balanced Lewis acid–base pairs was masked by the coexisting Brønsted acidity in the aldolization and self-deoxygenation of acetone to isobutene. As a result, $Zn_xZr_yO_z$ catalysts with only Lewis acid–base pairs were discovered, on which nearly a theoretical selectivity to isobutene (~88.9%) was successfully achieved, which has never been reported before. Moreover, the absence of Brønsted acidity in such $Zn_xZr_yO_z$ catalysts also eliminates the side isobutene isomerization and undesired polymerization/coke reactions, resulting in the production of high purity isobutene with significantly improved catalyst stability (<2% activity loss after 200 h time-on-stream). This work not only demonstrates a balanced Lewis acid–base pair for the highly active and selective cascade ethanol-to-isobutene reaction but also sheds light on the rational design of selective and robust acid–base catalyst for C–C coupling via aldolization reaction.

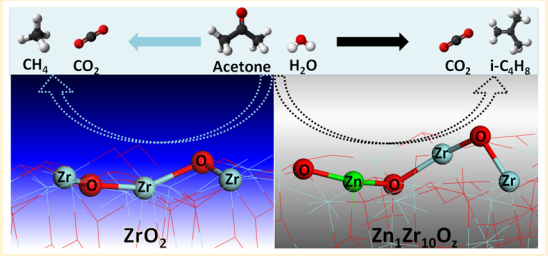

1. INTRODUCTION

As one of the most important olefins, isobutene has found wide applications in the production of industrial commodities such as butyl rubber and ethyl *tert*-butyl ether (ETBE).[1] Currently, the majority of isobutene is produced by steam cracking of naphtha. This process is energy-intensive and produces a mixture of different C_4 isomers, and a further separation of isobutene from the C_4 isomers is required to obtain high purity isobutene. Together with dwindling fossil fuel resources, it is desirable to explore sustainable feedstock to produce high purity isobutene.

Acetone aldolization and further self-deoxygenation have been widely studied to produce isobutene on zeolite catalysts with Brønsted acidity at high temperatures (>350 °C).[2−7] The surface Brønsted acid site has been proposed to protonate acetone to form enol/enolate intermediate, which then reacts with another acetone to produce diacetone alcohol via aldol addition.[8,9] Diacetone alcohol then dehydrates to form mesityl oxide that decomposes to isobutene and acetic acid (Scheme 1).[2] The main disadvantage of acetone-to-isobutene reaction on zeolites is the strong Brønsted acid-catalyzed secondary reaction of intermediates and isobutene to aromatics, other hydrocarbons, and coke (Scheme 1).[10] This leads to the rapid deactivation of zeolite catalysts.[3,11] Although alkaline metal ions have been used to tune activity and improve stability,[3] the isobutene yields are low (~55%), with notable deactivation within 10 h of time-on-stream.

Lewis acid–base pairs of (mixed) metal oxide have also been found highly active in the aldolization of acetone,[10,12−20] which mainly resulted in oxygenated adducts such as diacetone alcohol, mesityl oxide, and phorone, etc. Surface chemistry of acetone on Lewis acid–base site has been well understood, based largely on the IR probing of adsorption mode and identification of reaction species at both low[13] and high temperature.[19,21−23] It is generally accepted that the Lewis acid–base pair plays a concerted role in the acetone aldolization. Specifically, acetone is adsorbed on Lewis acid sites, while H abstraction from the α-methyl group occurs on the adjacent basic oxygen to form an enol/enolate

Received: July 15, 2015
Published: December 1, 2015

DOI: 10.1021/jacs.5b07401
J. Am. Chem. Soc. 2016, 138, 507−517

Scheme 1. Reported Acetone Reaction Network on Brønsted Acid and Lewis Acid–Base Pair

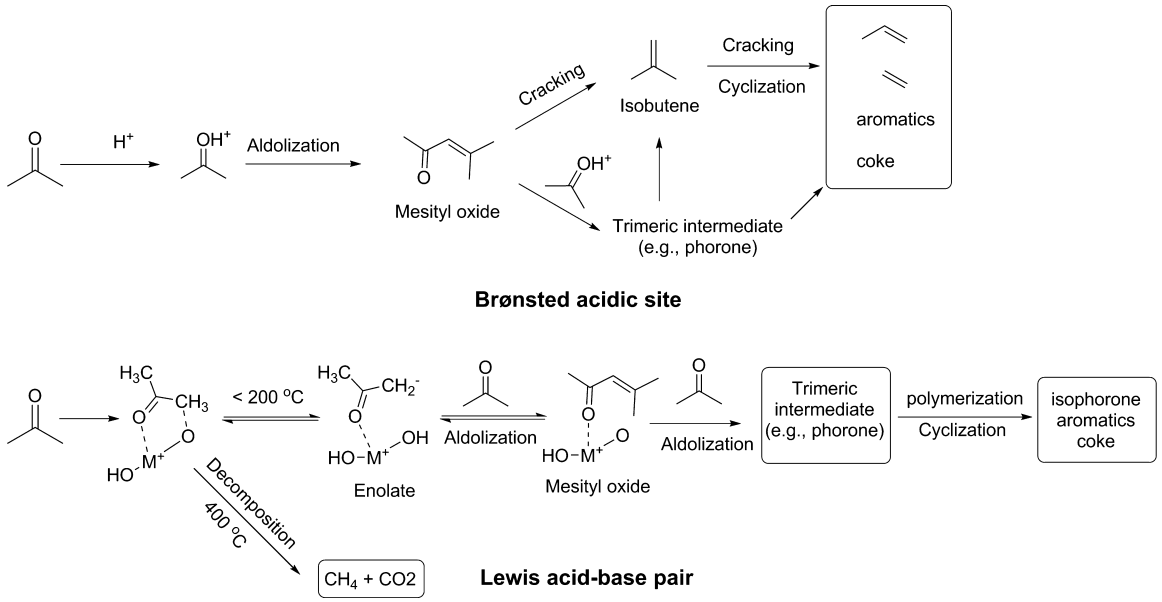

intermediate.[12] The enol/enolate intermediate then reacts with another acetone to form mesityl oxide, trimeric intermediates (e.g., phorone), and even aromatics via a complex condensation and cyclization reactions at temperatures <200 °C (Scheme 1). At high temperature (>300 °C), however, a parallel decomposition reaction is triggered by the oxidative surface basic hydroxyl groups and cus O^{2-}, leading to the dominant decomposition products (i.e., methane and CO_2) albeit minor isobutene formation. Using *in situ* IR, Zaki et al.[21] studied surface reaction of acetone at temperatures ranging from room temperature to 400 °C over a variety of metal oxides (e.g., TiO_2, ZrO_2, and CeO_2). It was found that aldolization readily took place at temperatures <200 °C, while the oxidation ability of surface hydroxyl groups became significant at high temperatures above 300 °C on Lewis acid–base pair, leading to the dominant acetone decomposition (Scheme 1).

We recently reported that $Zn_xZr_yO_z$ mixed oxides synthesized using a hard template (denoted as $Zn_xZr_yO_z$-H in this paper) have balanced surface acid–base properties, which are capable of catalyzing a cascade reaction from ethanol-to-isobutene via acetaldehyde and acetone intermediates at 450 °C.[24,25] It was found that sulfur in the BP-2000 hard template is incorporated into the $Zn_xZr_yO_z$-H catalysts after removing the hard template via calcination,[26] leading to the formation of strong Brønsted acid sites in addition to Lewis acid sites. ZnO addition can suppress most of the strong Brønsted acid sites and introduce basic sites, shifting the reaction pathway from ethanol dehydration to ethanol dehydrogenation and ketonization pathway toward acetone, followed by a rate-limiting acetone-to-isobutene reaction catalyzed by weak Brønsted acid sites.[24,25] Very recently, a similar $Zn_xZr_yO_z$ catalyst with weak Brønsted acid sites was also reported by Crisci et al. for a cascade acetic acid to isobutene reaction.[27] Unfortunately, $Zn_xZr_yO_z$-H catalysts with Brønsted acidity suffer from rapid deactivation by losing active sites for the secondary acetone-to-isobutene reaction.[24] Given the results previously reported on the roles of Lewis acid–base pair and Brønsted acid site in the acetone-to-isobutene reaction,[13,20,25] we further studied the acid properties of $Zn_xZr_yO_z$-H catalysts. We particularly focus on the elucidation of the roles of acid type on the secondary rate-determining acetone conversion in the cascade ethanol-to-isobutene reaction. It was found that both Brønsted acid sites and Lewis acid–base pairs are active for the acetone aldolization and self-deoxygenation to produce isobutene. However, Brønsted acid site also catalyzes undesired isobutene isomerization reaction and coke formation, leading to the catalyst deactivation. In contrast, balanced Lewis acid–base pairs exhibit high activity and stability in the selective acetone-to-isobutene conversion.

2. EXPERIMENTAL SECTION

2.1. Materials and Catalyst Synthesis. $Zn(NO_3)_2{\cdot}6H_2O$ (Sigma-Aldrich, reagent grade, 98%), zirconium(IV) oxynitrate hydrate (Sigma-Aldrich, 99%), $Zr(OH)_4$ (MEL, XZO631/01), BP-2000 (carbon black pearl 2000, Cabot Corp.), ZnO (Sigma-Aldrich, >99.99%), ethanol (Pharmco-AAPER, 200 proof), acetone (J.T. Baker, 99.8%), acetone-d_6 (Sigma-Aldrich, 99.9%), pyridine (J.T. Baker, 100%), and diacetone alcohol (Sigma-Aldrich, 99%) were used as purchased. Two different methods were used to synthesize the $Zn_xZr_yO_z$ catalysts, namely the hard template method and simple incipient wetness impregnation without using hard template. The details for the hard template synthesis can be found elsewhere.[25,28] In this paper, all the catalysts synthesized via hard template method were denoted as $Zn_xZr_yO_z$-H. For the incipient wetness impregnation method, the $Zr(OH)_4$ was used as support and initially dried overnight at 105 °C to remove any excess water on the surface before impregnation. A $Zn(NO_3)_2$ solution was then added on $Zr(OH)_4$ to achieve wet impregnation. After impregnation, the catalysts were dried overnight at room temperature followed by 4 h at 105 °C. The catalysts were further heated to 400 °C (3 °C/min) and held for 2 h followed by a 5 °C/min ramp to the final calcination temperature (i.e., 550 °C) and held for 3 h. The catalysts synthesized using the incipient wetness impregnation are denoted as $Zn_xZr_yO_z$-I. High purity commercial ZnO was used directly. ZrO_2 was prepared by calcining $Zr(OH)_4$ and using same temperature program for the $Zn_xZr_yO_z$-I catalysts. The details of the sample notation and physical–chemical properties are summarized in Table 1.

2.2. Catalyst Characterization. *X-ray Diffraction (XRD).* XRD patterns were collected on a Philips X'pert MPD (Model PW 3040/00) equipped with a Cu Kα X-ray source operating at 40 kV and 50 mA. A scanning step of 0.04° and duration time of 1.6 s per step were used at 2θ = 10°–90° over all the catalysts.

DOI: 10.1021/jacs.5b07401
J. Am. Chem. Soc. 2016, 138, 507–517

Table 1. Notation and Physical−Chemical Properties of the (Mixed) Metal Oxides

	type of acidity[a]				
sample name	Brønsted	Lewis	surface area (m^2/g)	method of preparation	note
ZrO_2−H	√	√	138.0	hard template-BP2000	ref 25
$Zn_1Zr_{10}O_z$-H	√	√	124.0	hard template-BP2000	ref 25
ZrO_2	√ (minor)	√	89.0	calcined $Zr(OH)_4$	this work
$Zn_1Zr_{10}O_z$-I		√	91.0	impregnation-$Zr(OH)_4$	this work
ZnO		√	4.0	commercial ZnO	this work

[a]Identified by IR-Py.

Infrared Analysis of Adsorbed Pyridine/Acetone-d_6/D_2O/CO_2 (IR-Py/Acetone-d_6/D_2O/CO_2). IR-Py/acetone-d_6/D_2O/CO_2 spectra were recorded on a Bruker Tensor 27 FTIR spectrometer. About 20 mg of the catalyst was loaded into an *in situ* cell and pretreated at 450 °C for 1 h under flowing helium at 50 sccm. The sample was cooled to 50 °C prior to taking a background or sample scan. For the IR-D_2O experiment, background was taken on KBr at 50 °C. Probe molecules (i.e., pyridine or acetone-d_6 or D_2O) were introduced by flowing He (10 sccm) through an ice-cooled bubbler for 10 min, during which the surface was saturated as confirmed by IR. For CO_2 adsorption, 50 sccm of 10% CO_2/He was flowing through the catalyst until the surface was saturated as confirmed by IR. The sample was then purged for 30 min using 50 sccm He to remove any physisorbed molecules. A spectrum was then taken at 50 °C. The sample was then ramped at 10 °C/min to a given temperature, which was followed by a 30 min purge at the elevated temperature before being cooled to 50 °C and scanned. Spent $Zn_1Zr_{10}O_z$-H catalyst used for IR-Py measurements was generated as follows. Prior to the IR experiment, reaction was first performed under reaction conditions until the end of the induction period was identified by GC analysis. After that the catalyst was cooled down to room temperature in N_2 flow for IR experiment. A mixture of spent $Zn_1Zr_{10}O_z$-H and KBr (1/5 weight ratio) was used to achieve a better signal-to-noise ratio.

Temperature-Programmed Desorption of Ammonia (NH_3-TPD). NH_3-TPD was carried out in a Micromeretics Autochem 2920. About 100 mg of sample was loaded and pretreated with a 10 °C/min ramp to 550 °C and held for 60 min. Ammonia was flowed over the sample at 50 °C until it was fully saturated, at which point it was purged in helium to remove any physisorbed ammonia. The sample was then ramped to 700 °C at 20 °C/min, and the signals were monitored using mass spectroscopy (ThermoStars GSD 320) calibrated by decomposition of a calculated amount of ammonium oxalate monohydrate. Quantification of Lewis acid sites is summarized in Table 2.

Nitrogen Sorption. Nitrogen sorption experiments were carried out at liquid nitrogen temperatures (−196 °C) on the Micromeretics TriStar 2 3020 physisorption analyzer. Prior to measurement, samples were degassed at 350 °C for 3 h under vacuum.

2.3. Catalyst Evaluation. The catalysts were evaluated in a home-built test unit described elsewhere.[25] Briefly, a given amount of catalyst was loaded into a microtubular fixed-bed reactor (i.d. 5 mm) and pretreated at 450 °C with 50 sccm N_2 for 30 min. An ethanol (or acetone or diacetone alcohol)/water solution with steam-to-carbon molar ratio (S/C) of 5 is typically used unless otherwise stated. The solution was fed to an evaporator at 150 °C and carried into the reactor by flowing N_2. Products were analyzed online using a Shimadzu GC-2014 gas chromatograph (GC) equipped with an autosampling valve, HP-Plot Q column (30 m, 0.53 mm, 40 μm), flame ionization detector (FID), and thermal conductivity detector. The product stream was then fed through a condenser, and the dry gases were sent to an online Agilent 490 MicroGC equipped with four heated blackflush channels (MSSA, PPQ, AL_2O_3/KCL, 5CB) for analysis. Equations 1 and 2 show the ideal reaction for ethanol-to-isobutene and acetone-to-isobutene. Based on the two equations, the theoretical carbon selectivity to isobutene ($S_{t\text{-}IB}$) for ethanol-to-isobutene and acetone-to-isobutene are 66.7% and 88.9%, respectively.

$$3CH_3CH_2OH + H_2O \rightarrow i\text{-}C_4H_8 + 2CO_2 + 6H_2 \quad (1)$$

$$3CH_3COCH_3 \rightarrow 2i\text{-}C_4H_8 + CO_2 + H_2O \quad (2)$$

For the kinetic acetone/H_2O and acetone-d_6/D_2O reactions, 10−400 mg of catalyst was loaded, and the space velocity was varied to control the acetone conversion from 5% to 20%. The rate was calculated based on the Lewis acid sites measured by NH_3-TPD.

For the controlled acetone/H_2O experiments with preadsorbed carbonate and acetate species, the preadsorption of carbonate and acetate was conducted by replicating the same procedure for IR-acetone experiments. Specifically, 10.5 mg of the catalyst (diluted with 490 mg of SiC) was loaded into the reactor and pretreated at 450 °C for 1 h under flowing nitrogen at 50 sccm. The catalyst was then cooled down to 50 °C where acetone adsorption was conducted by flowing the 0.47 mol % acetone in N_2 for 5 min. After the acetone adsorption, the catalyst was purged with flowing N_2 (50 sccm) for 30 min and then ramped to 450 °C in N_2 (50 sccm), where the acetone/H_2O steady-state reaction was performed.

Acetone/ethanol conversion (X_r), product selectivity ($S_{products\text{-}i}$), and isobutene theoretical yield (Y_{IB}) were calculated as follows: $X_r = (mol_{reactant\text{-}in} - mol_{reactant\text{-}out})/mol_{reactant\text{-}in}$; $S_{products\text{-}i} = (mol_{product\text{-}i} \times \alpha_i)/(mol_{reacted\ reactant} \times \beta)$, where α_i and β refers to the carbon number in product-i and reactant, respectively; $Y_{IB} = X_{products\text{-}i}/S_{t\text{-}IB}$.

3. RESULTS AND DISCUSSION

3.1. Physical−Chemical Properties of the Catalyst. Both physical and chemical properties of $Zn_xZr_yO_z$-H have been described elsewhere[25] and are summarized in Table 1. BET surface areas of the $Zn_xZr_yO_z$-I catalysts are also shown in Table 1. ZrO_2 and $Zn_1Zr_{10}O_z$-I show comparable surface area of ∼90 m^2/g. Commercial ZnO exhibits a low surface area of 4 m^2/g. XRD patterns of the $Zn_xZr_yO_z$-I are shown in Figure 1. A mixture of tetragonal and monoclinic ZrO_2 phases is detected on ZrO_2 prepared by calcination of $Zr(OH)_4$ at 550 °C. With Zn addition, tetragonal ZrO_2 is resolved by XRD after calcination at 550 °C. When the Zn/Zr ratio is between 1/6 and 1/14, no diffraction peak characteristic of ZnO but only tetragonal ZrO_2 phase is detected on $Zn_xZr_yO_z$-I. This suggests that ZnO is highly dispersed and inhibits the phase transition of

Table 2. Acetone Aldolization and Decomposition Rate Constant on the (Mixed) Metal Oxides

		decomposition rate constant[b]			aldolization rate constant[b]		
catalyst	Lewis acid site[a] (mmol/g)	k_{decomp}	k_{decomp}'	KIE_{decomp}	k_{aldol}	k_{aldol}'	KIE_{aldol}
ZrO_2	0.443	1.47	1.35	1.1	0.13	0.13	1.0
$ZnZr_{10}O_{z\text{-}I}$	0.319	1.39	1.34	1.0	26.50	25.44	1.0
ZnO	0.015	0.49			5.15		

[a]Number of Lewis acid site is quantified by NH_3-TPD. [b]Rate is normalized by the number of the Lewis acid site; k for acetone/H_2O reactions; k' for acetone-d_6/D_2O reactions

DOI: 10.1021/jacs.5b07401
J. Am. Chem. Soc. 2016, 138, 507−517

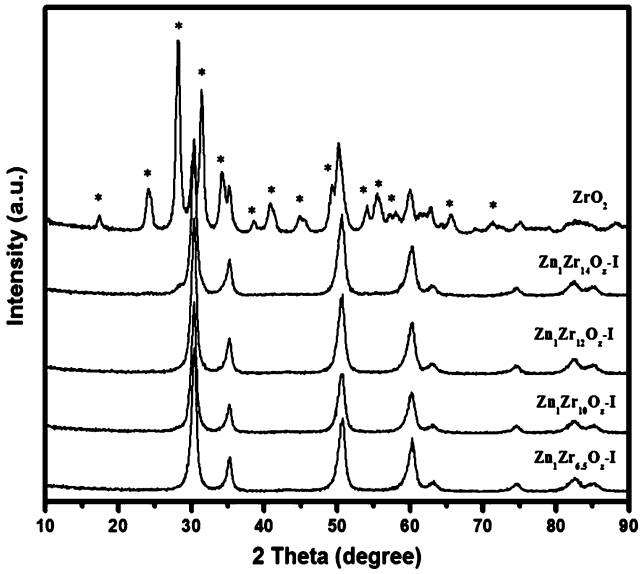

Figure 1. XRD patterns of ZrO_2 and $Zn_xZr_yO_z$-I catalysts. Asterisk marks the monoclinic phase.

ZrO_2 from tetragonal to monoclinic phase. Interestingly, IR spectra of both ZrO_2 and $Zn_xZr_yO_z$-I mixed oxides (Figure 2)

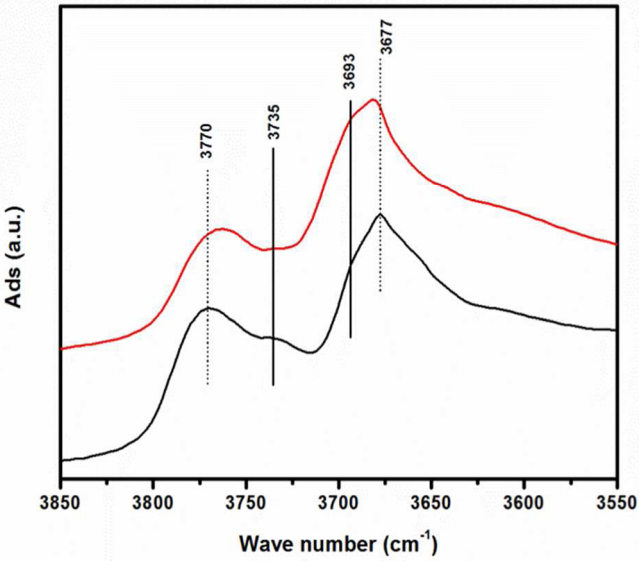

Figure 2. DRIFTS analysis of surface hydroxyl groups on ZrO_2 (black curve) and $Zn_xZr_yO_z$-I (red curve) catalysts. Catalysts were dehydrated at 450 °C for 1 h before IR collection. KBr was used as background.

display the pattern of surface hydroxyl groups that are identical to monoclinic ZrO_2.[29] This indicates that the surface of both catalysts is dominant by a thin layer of monoclinic ZrO_2 phase, which is beyond the detection limit of XRD. Similar behavior was also observed on other heteroatom (e.g., Y_2O_3)-doped ZrO_2.[30] It should be noted that the peak representing terminal (3770 cm^{-1}) and tribridged hydroxyl groups (3677 cm^{-1}) shifted to lower and higher wavenumbers after the addition of ZnO, an indication of change of the surface chemistry over $Zn_xZr_yO_z$-I.

IR spectra of adsorbed pyridine reveal strong Lewis acidity on ZrO_2 evidenced by the bands at 1604 and 1444 cm^{-1} (Figure 3). In addition, a weak band at 1540 cm^{-1} is also

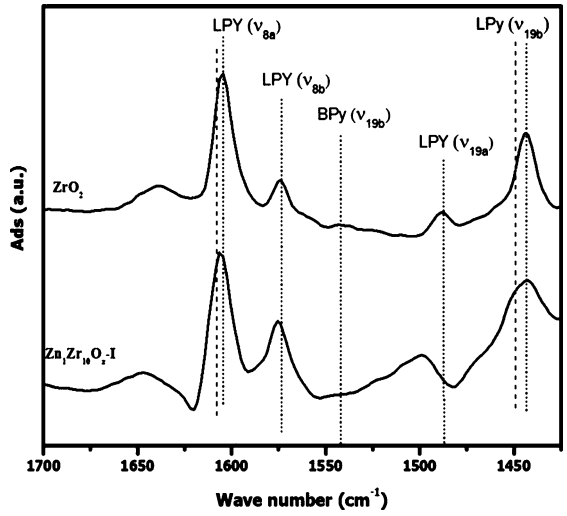

Figure 3. IR-Py of ZrO_2 and $Zn_xZr_yO_z$-I catalysts.

resolved which is identified as protonated Py species.[7,21] However, the intensity of this band is much weaker than that on ZrO_2 prepared using BP2000 carbon as a hard template (ZrO_2-H)[25] on which significant sulfur (1.3 wt %) was detected.[31] Given the fact that strong Brønsted acid sites could be generated on sulfated zirconia,[32] the weak Brønsted acid sites on ZrO_2 (Table 1) are likely from a S impurity on the $Zr(OH)_4$ precursor (<200 ppm). After addition of ZnO (i.e., $Zn_1Zr_{10}O_z$-I), however, only Lewis acidity is observed (Figure 3), which is consistent with the previous observation that ZnO can passivate Brønsted acid sites.[25] In addition, the peak associated with pyridine adsorbed on Lewis acid sites shifted to higher wavenumbers, suggesting the strength of the Lewis acidity becomes weaker.[25] The weakened Lewis acidity can be further confirmed by our theoretical calculations (section 3.5). The surface basicity of the catalysts was also investigated using IR-CO_2 experiments, as shown in Figure S1. It was found that after the addition of ZnO on ZrO_2 (i.e., $Zn_1Zr_{10}O_z$-I) the strength of both surface Lewis acid−base pairs and basic cus O^{2-} increased signficantly, evidenced by the experiments at different desorption temperatures. It suggests that the addition of ZnO weakened surface Lewis acidity and improved basicity, leading to the balanced acid−base properties on the $Zn_1Zr_{10}O_z$-I.

3.2. Acetone Reaction on $Zn_xZr_yO_z$-H. In our previous work, different residence time experiments reveal that acetone acts as the key intermediate in ethanol-to-isobutene, and the reaction is limited by the acetone-to-isobutene conversion.[25] Further durability tests on $Zn_1Zr_{10}O_z$-H catalysts show that IB selectivity decreases slowly with time-on-stream; meanwhile, acetone selectivity increases.[24] However, the selectivity to acetone and IB remains constant, suggesting that the catalyst loses active sites for the secondary acetone reaction during the ethanol-to-isobutene.[24] To better understand the deactivation mechanism, we investigate the acetone-to-isobutene rate-determining reaction on the catalysts with different type of acidity.

3.2.1. Acetone Reaction on $Zn_1Zr_{10}O_z$-H. Figure 4 shows the acetone-to-isobutene reaction over the $Zn_1Zr_{10}O_z$-H catalyst with Zn/Zr ratio optimized for ethanol-to-isobutene.[25] Acetone conversion initially increases with time-on-stream. After 10 h time-on-stream, it decreases monotonically with time-on-stream due to the loss of active sites observed in

DOI: 10.1021/jacs.5b07401
J. Am. Chem. Soc. 2016, 138, 507−517

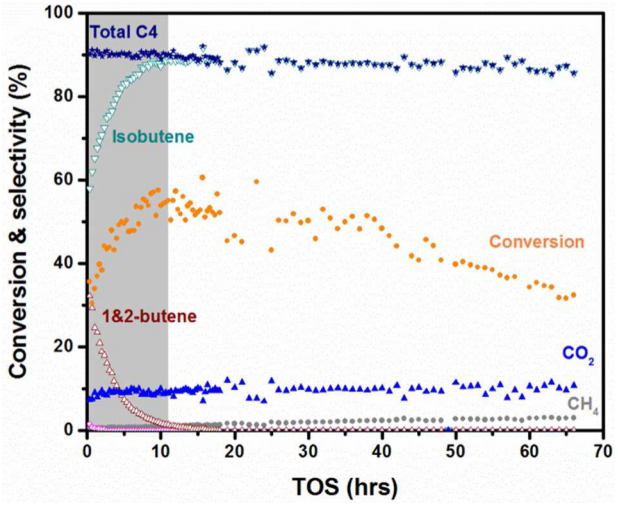

Figure 4. Acetone to isobutene reaction on $Zn_1Zr_{10}O_z$-H. 100 mg of catalyst, $P_{acetone}$ = 0.47 kPa, S/C = 5, T = 450 °C, WHSV = 0.37 $g_{acetone}$ g_{catal} h^{-1}.

ethanol-to-isobutene reaction. Significantly, there is an induction period during which acetone conversion increases with time-on-stream (time-on-stream <10 h). In addition, appreciable amounts of 1- and 2-butenes (~32%) are formed initially at the expense of isobutene. With time-on-stream, selectivity toward 1- and 2-butenes decreases rapidly with the concurrent increase of isobutene selectivity. However, selectivity to total $C_4^=$ olefins (1-butene, 2-butene, and isobutene) is high and remains constant (~89.0%). After the induction period, selectivity to 1- and 2-butenes decreases to zero, and selectivity to isobutene reaches ~89%, which is close to the theoretical selectivity (i.e., ~88.9%). Such dramatic changes in product distribution during the induction period are likely related to the evolution of catalyst surface properties.

Brønsted acidity has previously been identified as an active site for the acetone-to-isobutene reaction.[24,25] To better correlate product selectivity with catalyst surface properties, we further investigated the surface acidity of the fresh catalyst and spent catalyst right after the induction period using IR spectra of adsorbed pyridine (Figure 5). Over the fresh $Zn_1Zr_{10}O_z$-H catalyst (Figure 5A), both Lewis (1451, 1574, and 1608 cm^{-1}) and Brønsted acid sites (1544 cm^{-1}) are observed at a desorption temperature of 150 °C. Upon increasing the desorption temperature, pyridine adsorbed on Lewis and Brønsted acid sites decreases. However, pyridine adsorbed on Brønsted acid sites decreases more profoundly. At 450 °C, while most pyridine on Brønsted acid sites have desorbed, those adsorbed on Lewis acid sites are still observed in substantial amount, suggesting stronger Lewis acidity is present on the catalyst.

Over the spent $Zn_1Zr_{10}O_z$ catalyst right after the induction period (Figure 5B), the peaks characteristic of both Lewis (1451 and 1608 cm^{-1}) and Brønsted acid sites (1544 cm^{-1}) are still present at a desorption temperature of 150 °C. However, the shoulder peak at 1445 cm^{-1} (characteristic of strong Lewis acid sites on ZrO_2) almost disappears. More importantly, the relative area ratio of the integrated peak representing Brønsted acid sites at 1550 cm^{-1} (A_{1550}) to that of Lewis acid sites at 1450 cm^{-1} (A_{1450}) changes significantly. At a desorption temperature of 150 °C, the A_{1550}/A_{1450} decreases from 0.24 to 0.029, indicating that the surface Brønsted acid sites reduce rapidly during the induction period. It is well-known that Brønsted acid sites could catalyze the isomerization of $C_4^=$.[33] Considering the conversion of isobutene to butenes is thermodynamically favorable at high temperature (e.g., 450 °C in this case),[34] the constant and high selectivity to $C_4^=$ coupled with decreasing 1- and 2-butene/isobutene ratio with diminished Brønsted acid sites suggest that Brønsted acid sites catalyze isomerization of isobutene to form 1- and 2-butene. The Brønsted acid sites could also catalyze other polymerization side reactions, leading to coke deposition and thus loss of Brønsted acid sites on the catalyst.

Unexpectedly, acetone conversion increases with decreased Brønsted acid site, which is contradictory with the hypothesis that Brønsted acid sites are active for acetone conversion to isobutene. While it is still unclear what role the Brønsted acid site plays in acetone-to-isobutene, a more active and stable phase must be present on the $Zn_1Zr_{10}O_z$-H catalyst. This phase is believed to be the Lewis acid–base pairs, supported by the IR-Py results of the spent $Zn_1Zr_{10}O_z$-H catalyst. In addition, methane and CO_2 selectivities increase slowly at the expense of isobutene with time-on-stream, which could be due to the slightly favorable acetone decomposition on the Lewis acid–

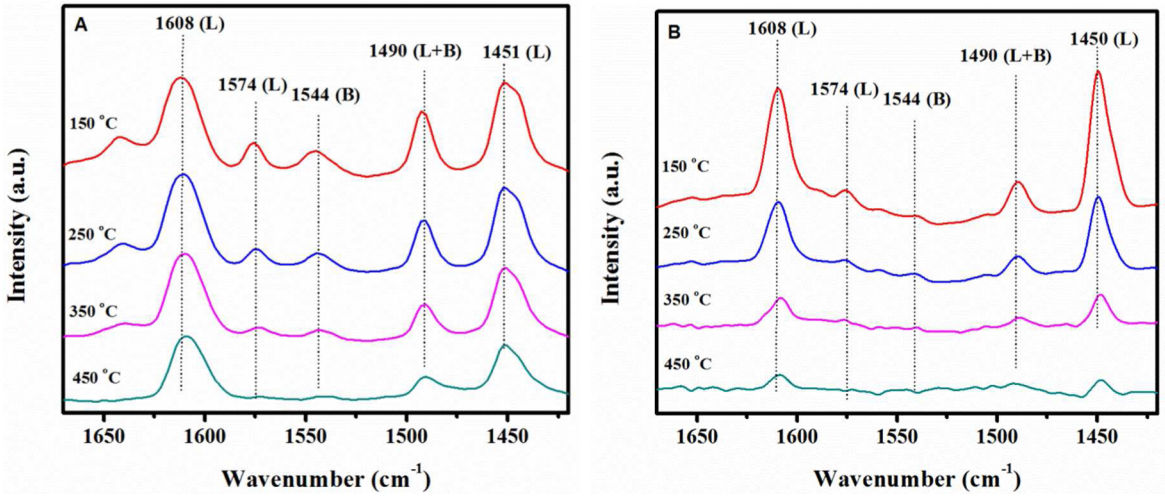

Figure 5. IR-Py of (A) fresh $Zn_1Zr_{10}O_z$-H and (B) spent $Zn_1Zr_{10}O_z$-H right after induction period at various desorption temperatures.

DOI: 10.1021/jacs.5b07401
J. Am. Chem. Soc. 2016, 138, 507–517

base pair. The activity for acetone condensation and decomposition on Lewis acid−base pairs is further discussed in section 3.3. It should be noted that Brønsted acid site is indeed active for acetone-to-isobutene, which will be confirmed in section 3.2.2. Given the fact that both Bronsted acid sites and Lewis acid−base pairs are active, a decrease in acetone conversion is expected with the loss of Brønsted acid sites. However, an increase in acetone conversion was observed. We speculate that the existence of both Brønsted acid (proton) and Lewis acid−base could affect each other. The proton generated from water dissociation on the strong Lewis center of the $Zn_xZr_yO_z$-H catalyst could be possibly stabilized by the basic oxygen of the Lewis acid−base pair (Scheme S1), inhibiting the activity of the Lewis acid−base pair by suppressing the α-H abstraction, a key step for acetone aldolization. After the induction period, the strong Lewis center that generates the protons could be passivated by coking, releasing the Lewis acid−base pair after the consumption of the protons.

3.2.2. Acetone Reaction on ZrO_2-H. To further confirm the role of Brønsted acidity, the acetone reaction on the ZrO_2-H catalyst was studied, and the results are shown in Figure 6.

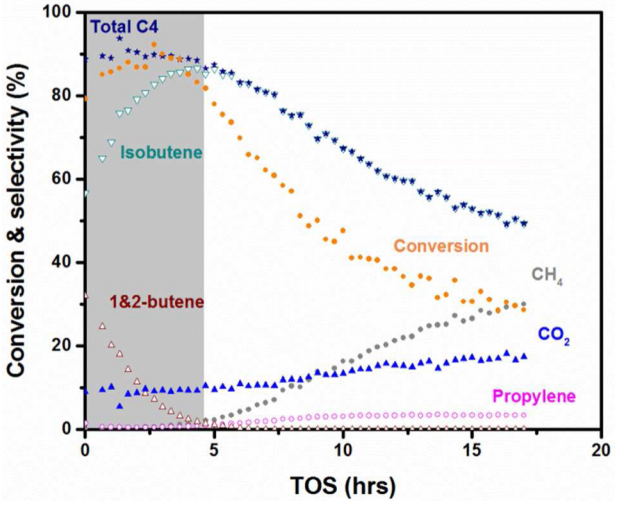

Figure 6. Acetone to isobutene reaction on ZrO_2-H. 100 mg, $P_{acetone}$= 0.47 kPa, S/C = 5, T = 450 °C, WHSV = 0.18 $g_{acetone}$ g_{catal} h^{-1}. Carbon balance is ∼80% during induction period and ∼71% afterward.

Since both Brønsted and Lewis acid sites are present on the ZrO_2-H catalyst as previously reported,[25] similar performances observed during the induction period for the $Zn_1Zr_{10}O_z$-H catalyst are expected for the ZrO_2-H catalyst. Indeed, a similar induction period, in which acetone conversion and isobutene selectivity increase while 1- and 2-butene selectivity decreases with time-on-stream, is also observed on the ZrO_2-H catalyst. After the induction period, however, acetone conversion and product distribution on the ZrO_2-H show totally different trends from those on $Zn_1Zr_{10}O_z$-H. Acetone conversion decreases dramatically with time-on-stream, and selectivity to methane and CO_2 increases rapidly at the expense of isobutene on ZrO_2. In addition, a small amount of propylene is also formed. These results suggest that Lewis acid−base chemistry on the ZrO_2-H is different from that on $Zn_1Zr_{10}O_z$-H.

Using FT-IR and mass spectrometry, Zaki et al.[21] studied acetone surface reaction on ZrO_2. It was found that acetone aldolization could occur on Lewis acid−base pairs at low temperature (<200 °C) to form mesityl oxide via diacetone alcohol intermediate. At high temperature (>350 °C), further cracking of mesityl oxide to isobutene was observed. Meanwhile, the surface hydroxyl group becomes very oxidative, catalyzing acetone decomposition and other reactions to form methane, CO_2, and propylene. Therefore, we believe that the increasing acetone decomposition is due to the loss of Brønsted acid sites and the emerging Lewis acid−base chemistry on the ZrO_2-H catalyst. The rapid deactivation together with the low carbon balance (∼71%) suggests that rapid coke formation and/or other side reactions also occur on the ZrO_2-H catalyst, likely due to the stronger Lewis acidity evidenced by IR-Py.[25] More importantly, the poor catalytic performance of Lewis acid−base pair on ZrO_2-H confirms that the high selectivity to isobutene in the induction period should be attributed to presence of Brønsted acid site during the acetone-to-isobutene reaction.

While it is still unclear why acetone conversion increases with diminished Brønsted acid active sites in the induction period on the $Zn_xZr_yO_z$-H catalyst, it does not affect our conclusion that Brønsted acid site is the active site for acetone aldolization toward isobutene production. Nevertheless, Brønsted acidity also favors secondary isobutene isomerization reaction to form 1- and 2-butene, and polymerization reactions (e.g., $C_4^=$ olefins and other intermediates such as mesityl oxide) to form coke with time-on-stream, which is further confirmed by the isobutene reactions on the $Zn_1Zr_{10}O_z$-H catalyst (Figure S2). Coke deposition on Brønsted sites leaves only Lewis acid−base pair on $Zn_1Zr_{10}O_z$-H, which is more active for acetone conversion but does not catalyze isobutene isomerization (Figure S2). The strong Lewis acid−base pairs on ZrO_2 also likely catalyze undesired acetone decomposition and coke formation reactions. Addition of ZnO to ZrO_2-H possibly neutralizes these stronger Lewis acid sites and introduces basic sites, leading to a highly active and selective catalyst for the acetone-to-isobutene reaction.

3.3. Acetone and Acetone-d_6 Reaction on $Zn_xZr_yO_z$-I.

Given the proposed functions of Lewis acid−base pairs and the detrimental effect of Brønsted and stronger Lewis acid sites in the acetone-to-isobutene reaction, the $Zn_xZr_yO_z$-I catalyst was synthesized to improve the selectivity and stability in acetone-to-isobutene reaction. Py-IR confirmed that only Lewis acid−base pairs are present (Figure 3). The acetone reaction was studied to validate that Lewis acid−base pairs are highly active for acetone conversion to isobutene, while mitigating isobutene isomerization and undesired coke formation. For comparison purposes, ZrO_2 and ZnO were also studied. Figure 7A shows the catalysts' performance in terms of isobutene selectivity versus acetone conversion, and Figure 7B compares the product distribution at similar acetone conversion of ∼22−26%. As expected, isobutene selectivity is constantly lower than 20% over ZrO_2 (Figure 7A). The majority of decomposition products, methane and CO_2, are formed (Figure 7B). In addition, a notable amount of propylene (<1%) is also formed (Figure 7B). ZnO shows a relatively high selectivity to isobutene (Figure 7), but it exhibits significantly low activity, which gives an aldolization rate constant 5-fold lower than that of $Zn_1Zr_{10}O_z$-I (Table 2).

The addition of ZnO to ZrO_2, however, significantly changed the reaction pathway from acetone decomposition to aldolization and self-deoxygenation. Over the $Zn_1Zr_{10}O_z$-I catalyst, an isobutene selectivity of >80% is achieved. The isobutene selectivity can even reach up to its theoretical value (88.9%) at acetone conversion of ∼10%. Notably, no other $C_4^=$

DOI: 10.1021/jacs.5b07401
J. Am. Chem. Soc. 2016, 138, 507−517

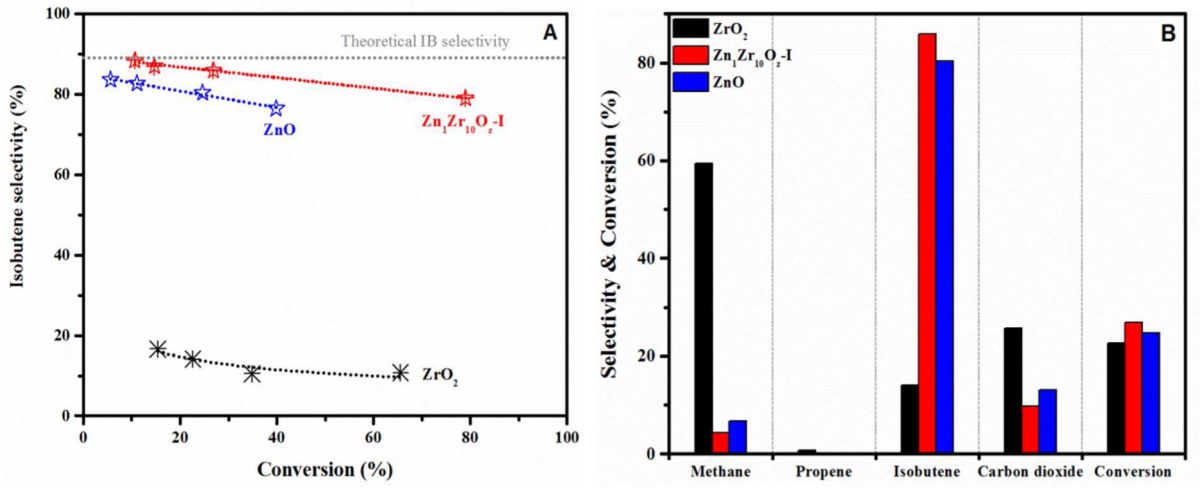

Figure 7. Isobutene selectivity versus acetone conversion (A) and products distribution at similar acetone conversion on mixed oxides (B). 10−400 mg, $P_{acetone}$ = 0.47 kPa, T = 450 °C.

isomers are observed, suggesting that the Lewis acid−base properties on $Zn_1Zr_{10}O_z$-I is very selective in isobutene production. In addition, the carbon balance is consistently higher than 95% on the $Zn_1Zr_{10}O_z$-I catalyst as opposed to $Zn_xZr_yO_z$-H (~85%), further confirming that side reactions (e.g., coking) observed in the presence of Brønsted acidity on $Zn_xZr_yO_z$-H are mitigated.

It is worth mentioning that selectivity to decomposition products (i.e., methane and CO_2) increases at the expense of isobutene as acetone conversion increases, likely due to kinetic inhibition of the aldolization reaction by adsorbed intermediate/product.

It is proposed that over $Zn_1Zr_{10}O_z$-I ZnO addition could either modify Lewis acid−base properties or suppress the oxidation capability of hydroxyl groups on the ZrO_2, leading to the relatively favorable acetone aldolization and self-deoxygenation toward isobutene formation. To confirm this hypothesis, kinetic analysis was performed (Figure S3), and the rate constants (k) are listed in Table 2. k_{decomp} for acetone decomposition (1.47) is more than a factor of 10 higher than k_{aldol} for acetone aldolization (0.13) on ZrO_2, suggesting acetone decomposition dominates on this catalyst. After the addition of ZnO (i.e., $Zn_1Zr_{10}O_z$-I), k_{decomp} decreases slightly from 1.47 to 1.39. However, k_{aldol} increases dramatically up to 26.50. The k_{aldol}/k_{decomp} ratio on $Zn_1Zr_{10}O_z$-I is 2 orders of magnitude higher than that on ZrO_2 (19.1 vs 0.1). Apparently, ZnO addition mainly modifies Lewis acid−base properties, leading to enhanced acetone aldolization and self-deoxygenation reaction and, thus, isobutene selectivity. It should be mentioned that despite the low k_{decomp} on ZnO, its k_{aldol} is also much lower than that of $Zn_1Zr_{10}O_z$-I (Table 2). It can be concluded that Lewis acid−base pair on the $Zn_1Zr_{10}O_z$-I is essential for high acetone aldolization rate.

To further understand the reaction mechanism, acetone-d_6/D_2O reaction was also studied on both ZrO_2 and $Zn_1Zr_{10}O_z$-I catalysts. Kinetic isotopic effects (KIEs) for the acetone decomposition and aldolization pathway were measured (Table 2) to identify if α-H abstraction and H_2O dissociation are the limiting steps in the cascade reactions. Over both $Zn_1Zr_{10}O_z$-I and ZrO_2 catalysts, a KIE from 1.0 to 1.1 was observed for acetone aldolization and decomposition pathway. It suggests that both the α-H abstraction and water dissociation are not the rate-determining step.

3.4. DRIFTS Analysis of Adsorbed Acetone-d_6. To further elucidate the roles of ZnO addition to ZrO_2 and possible reaction intermediates involved leading to improved isobutene selectivity, surface reaction of acetone-d_6 was further studied using *in situ* IR. The results are shown in Figure 8. The

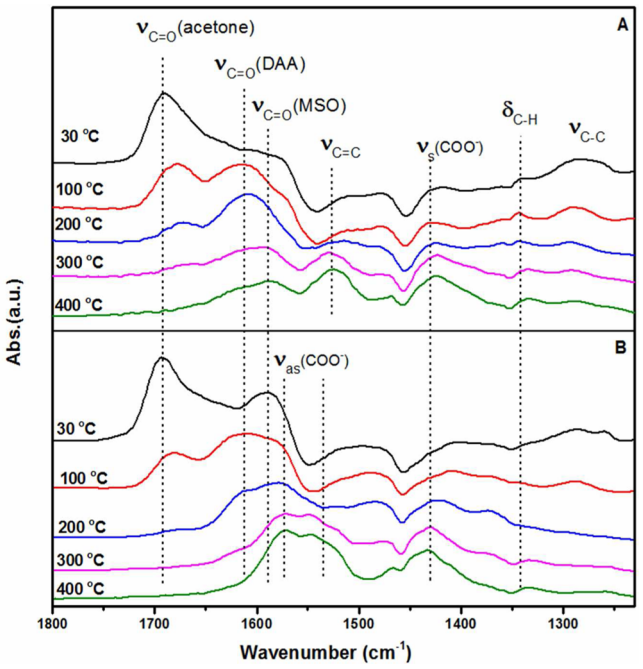

Figure 8. DRIFTS analysis of adsorbed acetone-d_6 over (A) ZrO_2-I and (B) $Zn_1Zr_{10}O_z$-I.

intent of using acetone-d_6 was to differentiate the activity for both α-H abstraction and aldolization. Figure 8A compares the IR spectra of acetone-d_6 adsorbed on ZrO_2 at different temperatures. At 30 °C, the νC═O/νC═C/νC−C/δC−H region give a strong band at 1691 cm^{-1}, a broad shoulder centered at ~1604 cm^{-1}, two weak bands at 1467 and 1343 cm^{-1}, and two moderate bands at 1288 and 1261 cm^{-1}. The strong band at 1691 cm^{-1} can be assigned to the νC═O of

DOI: 10.1021/jacs.5b07401
J. Am. Chem. Soc. 2016, 138, 507−517

acetone adsorbed on Lewis acid site,[21] which is further supported by the νC−C band at 1288 and 1261 cm^{-1}. The broad shoulder at 1604 cm^{-1} could have originated from the νC═O absorption of adduct species (i.e., diacetone alcohol and mesityl oxide) due to the minor aldol condensation of acetone.[21] The weak bands at around 1467 and 1343 cm^{-1} are due to the δC−H of adsorbed species (i.e., acetone, diacetone alcohol, and enol) formed from surface H−D exchange reaction between acetone-d_6 and surface hydroxyl groups,[14,35] In the νO−D and νC−D region, νC−D bands are observed at 2225, 2065, and 2138 cm^{-1} (Figure S4). Unfortunately, no νO−D bands are resolved, but instead, a broad hump at ∼2700 cm^{-1} is present due to hydrogen-bonded nature of OD groups.[14]

Upon increasing temperature, the bands corresponding to adsorbed acetone-d_6 (1691, 1288, and 1261 cm^{-1}) decrease significantly and disappear at temperatures above 300 °C. The decreasing acetone signal could be due to desorption and further conversion of acetone. The former can be confirmed by the separate acetone-TPD experiment, which shows acetone desorption at ∼110 °C (Figure S5). The latter is evidenced by the increased band intensity at 1612 cm^{-1}, characteristic of νC═O of diacetone alcohol coordinated to Lewis acid site, which first increases and then decreases with a maximum at 200 °C. Because of the significant oxidative nature of hydroxyl groups at high temperature,[21] most of diacetone alcohol could be quickly converted back to acetone[14] that decomposes (Scheme 2, red highlighted). This decomposition can be

Scheme 2. Proposed Acetone-to-Isobutene Reaction Mechanism over $Zn_xZr_yO_z$-I Catalyst

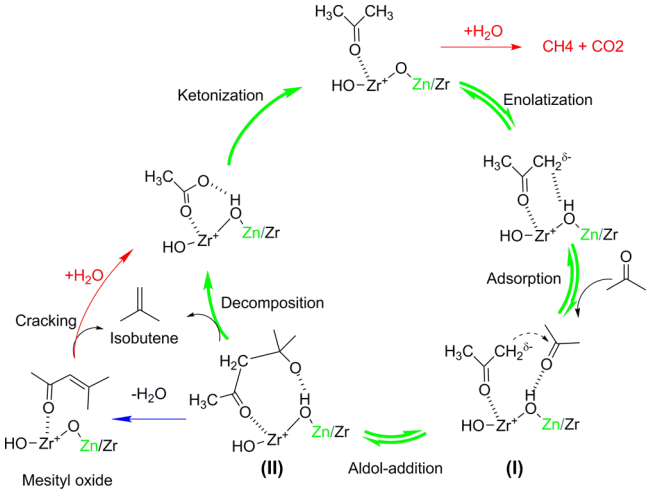

further confirmed by the significant decrease of intensity of all absorption bands (Figure 8A). Meanwhile, further dehydration of diacetone alcohol to mesityl oxide is also observed, evidenced by the further red-shift of νC═O band to 1595 cm^{-1}, νC═C absorption at 1525 cm^{-1}, νC−D bands at 2225 cm^{-1}, and δC−H band at 1343 cm^{-1}.[21] Notably, once mesityl oxide is formed, it is strongly adsorbed on the catalyst until 400 °C. Only minor mesityl oxide cracking occurs, evidenced by the shoulder bands of νCOO$^-$ of acetate species at 1575 cm^{-1} (antisymetric vibration) and 1430 cm^{-1} (symmetric vibration)[21] and that of carbonate species at 1550 and 1332 cm^{-1}.[29] It suggests that the strongly adsorbed mesityl oxide can block the Lewis acid site on ZrO_2, leading to the low aldolization activity. In addition, νO−D bands become resolved at 100 °C and increase with temperature (Figure S4), suggesting enhanced H−D scrambling between acetone-d_6 and surface hydroxyl at higher temperature.

Over $Zn_1Zr_{10}O_z$-I catalyst, other than the adsorbed acetone band at 1691 cm^{-1}, mesityl oxide bands at 1589 and 1525 cm^{-1} are also detected at 30 °C (Figure 8B), suggesting a facile aldolization pathway consistent with the kinetic results in section 3.3. As temperature increases, acetone intensity decreases due to the acetone desorption (Figure S5) and further reaction of acetone (Figure 8B). It should be mentioned that the extent of acetone desorption on ZrO_2 and $Zn_1Zr_{10}O_z$-I is almost identical (Figure S5). However, compared to that on ZrO_2, acetone intensity decreases more rapidly with temperature and disappears at a lower temperature (i.e., 200 °C), which further confirms the facile aldolization pathway on $Zn_1Zr_{10}O_z$-I. With the decrease of acetone, only a small amount of diacetone alcohol is observed at 100−200 °C. Mesityl oxide is always predominant on the $Zn_1Zr_{10}O_z$-I catalyst. Moreover, when temperature is above 300 °C (i.e., 400 °C), mesityl oxide decomposition seems significant, and only a small amount of mesityl oxide is left on the catalyst surface, evidenced by the very weak νC−D (2224 cm^{-1}), νC═O (1589 cm^{-1}), and νC═C (1525 cm^{-1}) bands. Instead, it is dominant with acetate and carbonate absorption, the former being assigned to the 1572, 1467, and 1430 cm^{-1} band and the latter to the 1547, 1446, 1432, and 1335 cm^{-1} ones.[21,29] This observation suggests that the forward diacetone alcohol dehydration to mesityl oxide and mesityl oxide cracking reactions are significantly enhanced relative to its reverse reaction to acetone on $Zn_1Zr_{10}O_z$-I (Scheme 2, green highlighted). This is consistent with the steady-state reaction data showing higher aldol-addition rate than that of decomposition. Unfortunately, the evolution of νO−D bands with temperature is difficult to differentiate from that of ZrO_2 (Figure S4) due to the interference (i.e., hydrogen bond) of strongly adsorbed acetate or carbonate species. It should be mentioned that the formation of carbonate and acetate species could block the surface active sites on the metal oxides (e.g., surface basic oxygen).[36−38] To verify if the surface identified acetate/carbonate will deactivate the catalyst or not, separate acetone reactions were performed on both fresh $Zn_1Zr_{10}O_z$-I and $Zn_1Zr_{10}O_z$-I with preadsorbed surface carbonate species (Figure S6). No obvious effect on the acetone has been observed, suggesting the surface carbonate does not deactivate the catalyst under the current reaction conditions consistent with the highly stable ethanol-to-isobutene reaction discussed in the section 3.6.

3.5. DRIFTS Analysis of Adsorbed D_2O. To further verify the H−D exchange reaction and water dissociation, D_2O-DRIFTS was performed on the two catalysts. Figure 9 displays the evolution of hydroxyl bands with desorption temperatures. Both isolated OH at 3770 cm^{-1} and tribridged OH at 3770 cm^{-1} are observed on the two freshly pretreated samples (gray line). Upon adsorption of D_2O at 50 °C, peaks characteristic of OH groups on both supports decrease significantly, and a broad hump at 3000−3400 cm^{-1}, characteristic of hydrogen-bonded OH, appears simultaneously. This suggests that the adsorbed D_2O interacts closely with hydroxyl groups via hydrogen bond. In addition, a new tribridged OD peak is observed on both ZrO_2 (2711 cm^{-1}) and $Zn_1Zr_{10}O_z$-I (2714 cm^{-1}). However, no isolated OD was observed. It indicates that no water dissociation occurs, but H−D exchange does take place on both catalysts.

DOI: 10.1021/jacs.5b07401
J. Am. Chem. Soc. 2016, 138, 507−517

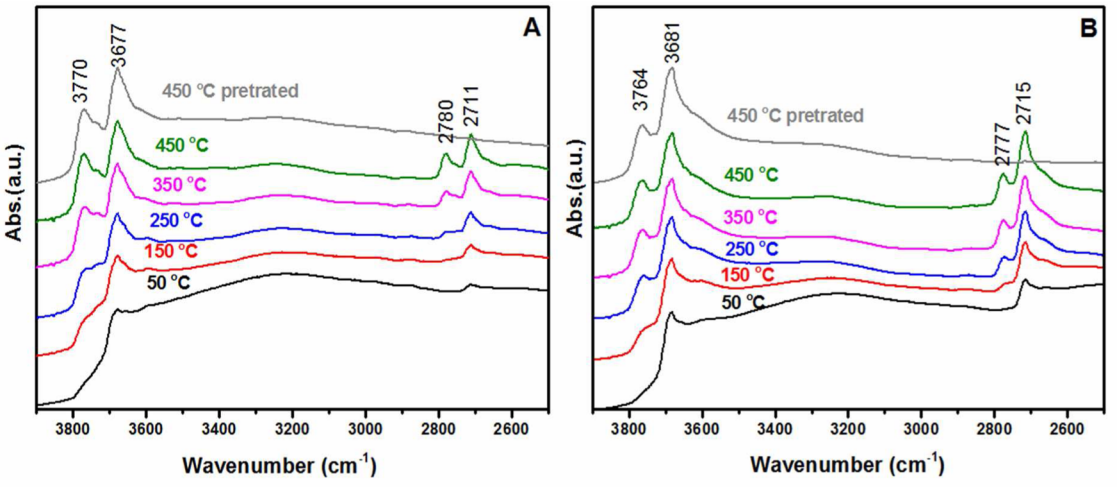

Figure 9. DRIFTS analysis of adsorbed D_2O on ZrO_2 (A) and $Zn_1Zr_{10}O_z$ (B).

The fact that the peak intensity for tribridged OD is higher on $Zn_1Zr_{10}O_z$-I than on ZrO_2 reveals that the H−D exchange reaction is more active for the former. As the temperature increases, hydrogen-bonded OH groups decrease as evidenced by the decreased intensity of the broad hump 3000−3400 cm^{-1}. Meanwhile, the peak of tribridged OD increases and isolated OD appears at 150 °C, suggesting enhanced H−D exchange and water dissociation might coexist. For a better comparison, the peak area representing the amount of OD bands is further integrated to explore the effect of temperature on the H−D exchange and water dissociation, as shown in Figure 10. As

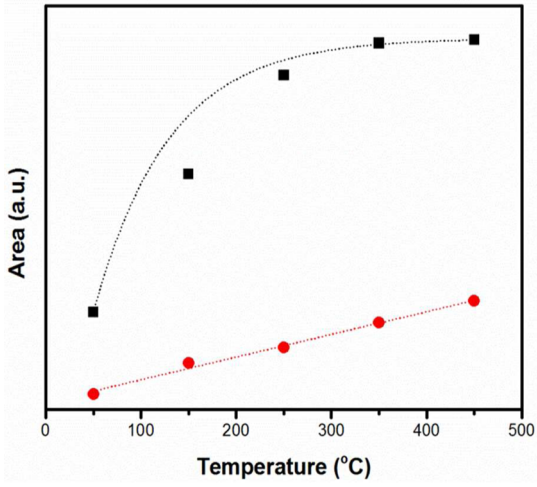

Figure 10. Evolution of the peak area with temperature representing OD groups on ZrO_2 (red) and $Zn_1Zr_{10}O_z$-I (black) shown in Figure 9.

temperature increases, it is clear that the amount of surface OD increases at a much faster rate on the $Zn_1Zr_{10}O_z$-I than that on ZrO_2. While the amount of OD increases monotonically as temperature is increased up to 450 °C, surface saturation appears to be achieved at >200 °C. It should be noted that the intensity of bands associated with OH groups also increase with temperature, which is due to the recovery of the OH groups from the hydrogen-bonded ones at 3000−3400 cm^{-1} since most of hydrogen-bonded D_2O is removed. At 450 °C, ∼25% and ∼10% of the OH groups have been exchanged on $Zn_1Zr_{10}O_z$-I and ZrO_2, respectively. It further confirms the facile H−D exchange on the $Zn_1Zr_{10}O_z$-I catalyst. Additionally, upon D_2O adsorption and treatment at 450 °C, the total OH groups on $Zn_1Zr_{10}O_z$-I and ZrO_2 increased by 1.51 and 1.55 times, respectively, assuming a OD/OH response ratio of 0.51.[39] The increased OH groups are attributed to the water dissociation that occurs on both $Zn_1Zr_{10}O_z$-I and ZrO_2 catalyst with the former being less active, which can be further confirmed by our theoretical calculations (Figure S7).

3.6. $Zn_1Zr_8O_z$-I Catalyst Stability for Ethanol-to-Isobutene. We have shown in our previous report that the $Zn_xZr_yO_z$-H (i.e., $Zn_1Zr_8O_z$-H) catalyst suffers deactivation in ethanol-to-isobutene due to the rapid loss of active sites for acetone-to-isobutene reaction. After 27 h, isobutene yield dropped from ∼79% to ∼61% with the concurrent increase of acetone.[24] Meanwhile, selectivities to other products were constant, suggesting that the catalyst is losing active sites for acetone-to-isobutene conversion. Given the high selectivity and stability of the balanced Lewis acid−base pairs in acetone-to-isobutene on the $Zn_xZr_yO_z$-I catalyst, we further evaluated the stability of $Zn_1Zr_8O_z$-I catalyst in terms of isobutene yield under similar reaction conditions (Figure 11). It is clear that the $Zn_1Zr_8O_z$-I catalyst shows extremely good stability in terms of

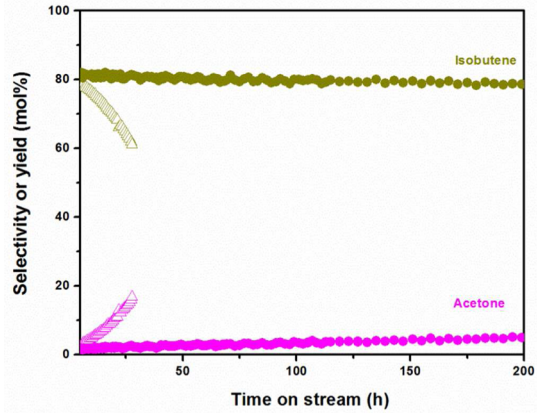

Figure 11. Stability test for ethanol-to-isobutene over $Zn_1Zr_8O_z$-I (solid mark). Dark yellow marked isobutene yield and magenta marked acetone selectivity. $P_{ethanol}$ = 83 kPa, S/C = 2.5, WHSV = 0.3 $g_{ethanol}$ g_{catal}^{-1} h^{-1}. T = 450 °C. For comparison, the ethanol-to-isobutene over $Zn_1Zr_8O_z$-H is also plotted (hollow marks).

DOI: 10.1021/jacs.5b07401
J. Am. Chem. Soc. 2016, 138, 507−517

isobutene selectivity. After 200 h time-on-stream, the loss in isobutene yield is very minor (less than 3%). Figure 12 shows

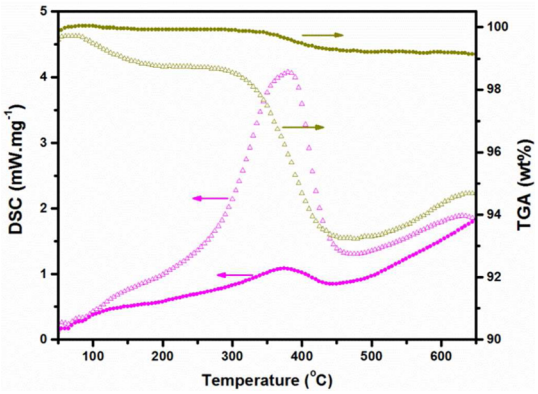

Figure 12. TGA (dark yellow)−DSC (magenta) analysis of spent $Zn_1Zr_8O_z$-I (solid mark). For comparison, the TGA−DSC over $Zn_1Zr_8O_z$-H is also plotted (hollow marks). Spent $Zn_1Zr_8O_z$-I was analyzed after 200 h time-on-stream. Spent $Zn_1Zr_8O_z$-H was analyzed after ∼27 h time-on-stream.

the thermogravimetric and differential scanning calorimetry (TG-DSC) analysis of the spent catalysts. Only ∼0.7 wt % coke was detected on $Zn_1Zr_8O_z$-I after 200 h of time-on-stream operations, whereas >5 wt % coke was observed on $Zn_1Zr_8O_z$-H after 27 h time-on-stream. It is clear that the balanced Lewis acid−base pairs are resistant to coke formation.

3.7. General Discussion. To the best of our knowledge, we first demonstrate a highly selective and stable acetone-to-isobutene conversion over $Zn_xZr_yO_z$-I catalysts with balanced Lewis acid−base pairs. A cascade aldolization and self-deoxygenation pathway is thus proposed in Scheme 2. The adsorbed acetone is stabilized on the $Zn_xZr_yO_z$-I by Lewis acid site while the neighboring basic oxygen is responsible for the α-H abstraction,[12] leading to the enolate species. Meanwhile, water dissociation and acetone decomposition to methane and CO_2 occur simultaneously (Scheme 2, red highlighted),[21] evidenced by IR-D_2O experiment (Figures 9 and 10), steady state reaction (Figure 7), and acetone/D_2O pulse reactions (Figure S8). The formed enolate species and another hydrogen-bonded acetone (I) then go through a nucleophlic addition reaction to form the adsorbed diacetone alcohol adduct (II). The diacetone alcohol adduct (II) could either decompose directly to form isobutene and a surface acetate or dehydrate to form an adsorbed mesityl oxide, which is then cracked to form isobutene and a surface acetate. To close the reaction loop, the two surface acetates are converted into another surface acetone via a facile ketonization. This hypothesis is further confirmed by our separate experiments on the $Zn_1Zr_{10}O_z$-I catalyst using acetic acid as reactant (Figure S9).

Over ZrO_2, from acetone/H_2O and acetone-d_6/D_2O kinetic studies, it reveals that the rate constant for the aldolization and self-deoxygenation cascade reaction is much lower than that for acetone decomposition on the Lewis acid base pair of ZrO_2 (1.47 vs 0.13), leading to its low selectivity during acetone-to-isobutene. The low activity for aldolization and self-deoxygenation is due to the strongly adsorbed mesityl oxide and thus blocked Lewis acid−base pair active site as evidenced by the DRIFTS analysis of adsorbed acetone-d_6 experiments. Upon addition of ZnO (e.g., $Zn_1Zr_{10}O_z$-I), the rate constant for acetone decomposition only decreased slightly from 1.47 to 1.39, whereas that for the cascade aldolization and self-deoxygenation reaction was improved by 2 orders of magnitude. This leads to the significantly increased selectivity toward isobutene. A comparison of acetone/H_2O and acetone-d_6/D_2O reactions showed no kinetic isotope effect on acetone decomposition on both ZrO_2 and $Zn_1Zr_{10}O_z$-I. This indicates that acetone decomposition is limited by C−C bond cleavage. However, the water dissociation must play the essential role in the acetone decomposition reaction (Scheme 2, red highlighted), which has been confirmed by our steady state acetone/H_2O reaction (Figure 7), IR-D_2O (Figure 9), and acetone/D_2O pulse reactions (Figure S8). On the other hand, no obvious kinetic isotope effect on the cascade acetone aldolization and self-deoxygenation reaction was observed, suggesting that α-H abstraction and hydrogen transfer is not the limiting step during the acetone aldolization. Instead, the cascade reaction must be limited by either the aldol addition or the subsequent reaction of surface adducts (II) to isobutene via either direct decomposition or mesityl oxide intermediate. To further confirm the reaction determining step, separate kinetic experiments were performed using diacetone alcohol as reactant as shown Figure S10. A rate constant of ∼21.73 was achieved for diacetone alcohol-to-isobutene, which is close to that of acetone-to-isobutene reaction (26.50, Table 2). This result suggests that the acetone-to-isobutene reaction is limited by the diacetone alcohol-to-isobutene reactions.

For the diacetone alcohol-to-isobutene conversion, it should be noted that water dissociation is involved in the secondary mesityl oxide cracking reactions (Scheme 2, blue highlighted). If adduct II goes through the mesityl oxide intermediate, an isotope effect should be observed in the acetone/H_2O and acetone-d_6/D_2O reactions on the $Zn_1Zr_{10}O_z$-I catalyst. The fact that no kinetic isotope effect on the aldolization was observed suggests that ZnO also promotes the direct conversion of adduct II, in which water dissociation is not involved. Indeed, our separate residence time experiments in Figure S11 indicate that isobutene was mainly produced by direct diacetone alcohol decomposition (>95%) in the diacetone-to-isobutene reactions.

4. CONCLUSION

Our results reveal that the Brønsted acid sites on the $Zn_xZr_yO_z$-H catalysts are indeed active for acetone-to-isobutene reaction. However, it also catalyzes isobutene isomerization reaction to form 1- and 2-butenes as well as other side reactions like polymerization and coke deposition on the catalyst. Lewis acid−base pairs on ZrO_2 catalyst can catalyze the acetone aldolization reaction to form mesityl oxide. The formed mesityl oxide strongly adsorbs and blocks the Lewis acid−base active site, resulting in the dominant acetone decomposition (Scheme 2, red highlighted pathway), as well as other possible side reactions like polymerization. However, ZnO addition significantly modifies the properties of surface Lewis acid−base pairs. As a result, the cascade acetone aldolization and self-deoxygenation reactions are significantly accelerated, leading to the highly active and stable $Zn_xZr_yO_z$-I catalyst for both acetone-to-isobutene and ethanol-to-isobutene. This work also demonstrates the importance of balancing the Lewis acid−base pairs to achieve a highly active and robust catalyst for cascade aldolization and self-deoxygenation reactions.

DOI: 10.1021/jacs.5b07401
J. Am. Chem. Soc. 2016, 138, 507−517

■ ASSOCIATED CONTENT

Supporting Information

The Supporting Information is available free of charge on the ACS Publications website at DOI: 10.1021/jacs.5b07401.

Figures S1−S11 and Scheme S1 (PDF)

■ AUTHOR INFORMATION

Corresponding Author

*E-mail: yong.wang@pnnl.gov (Y.W.).

Notes

The authors declare no competing financial interest.

■ ACKNOWLEDGMENTS

We acknowledge the financial support from the US Department of Energy (DOE), Office of Basic Energy Sciences, Division of Chemical Sciences, Geosciences, and Biosciences (DE-AC05-RL01830, FWP-47319), and Archer Daniels Midland Company (WSU002206). Computing time was granted by a user proposal at the William R. Wiley Environmental Molecular Sciences Laboratory (EMSL). EMSL is a national scientific user facility sponsored by the Department of Energy's Office of Biological and Environmental Research and located at the Pacific Northwest National Laboratory (PNNL).

■ REFERENCES

(1) Sun, J.; Wang, Y. *ACS Catal.* **2014**, *4*, 1078.
(2) Dolejsek, Z.; Novakova, J.; Bosacek, V.; Kubelkova, L. *Zeolites* **1991**, *11*, 244.
(3) Tago, T.; Konno, H.; Ikeda, S.; Yamazaki, S.; Ninomiya, W.; Nakasaka, Y.; Masuda, T. *Catal. Today* **2011**, *164*, 158.
(4) Chang, C. D.; Silvestri, A. J. *J. Catal.* **1977**, *47*, 249.
(5) Hutchings, G. J.; Johnston, P.; Lee, D. F.; Warwick, A.; Williams, C. D.; Wilkinson, M. *J. Catal.* **1994**, *147*, 177.
(6) Hutchings, G.; Johnston, P.; Lee, D.; Williams, C. *Catal. Lett.* **1993**, *21*, 49.
(7) Zhu, K.; Sun, J.; Liu, J.; Wang, L.; Wan, H.; Hu, J.; Wang, Y.; Peden, C. H. F.; Nie, Z. *ACS Catal.* **2011**, *1*, 682.
(8) Biaglow, A. I.; Sepa, J.; Gorte, R. J.; White, D. *J. Catal.* **1995**, *151*, 373.
(9) Xu, T.; Munson, E. J.; Haw, J. F. *J. Am. Chem. Soc.* **1994**, *116*, 1962.
(10) Salvapati, G. S.; Ramanamurty, K. V.; Janardanarao, M. *J. Mol. Catal.* **1989**, *54*, 9.
(11) Kubelková, L.; Čjka, J.; Nováková, J.; Boszácek, V.; Jirka, I.; Jíaru, P. In *Studies in Surface Science and Catalysis*; Jacobs, P. A., Santen, R. A. v., Eds.; Elsevier: 1989; Vol. *49*, p 1203.
(12) Iglesia, E.; Barton, D. G.; Biscardi, J. A.; Gines, M. J. L.; Soled, S. L. *Catal. Today* **1997**, *38*, 339.
(13) Panov, A. G.; Fripiat, J. J. *J. Catal.* **1998**, *178*, 188.
(14) Zhang, G.; Hattori, H.; Tanabe, K. *Appl. Catal.* **1988**, *40*, 183.
(15) Chheda, J. N.; Dumesic, J. A. *Catal. Today* **2007**, *123*, 59.
(16) Chen, Y. Z.; Hwang, C. M.; Liaw, C. W. *Appl. Catal., A* **1998**, *169*, 207.
(17) Nikolopoulos, A. A.; Jang, B. W. L.; Spivey, J. J. *Appl. Catal., A* **2005**, *296*, 128.
(18) Sanz, J. F.; Oviedo, J.; Márquez, A.; Odriozola, J. A.; Montes, M. *Angew. Chem., Int. Ed.* **1999**, *38*, 506.
(19) Quesada, J.; Faba, L.; Diaz, E.; Bennici, S.; Auroux, A.; Ordonez, S. *J. Catal.* **2015**, *329*, 1.
(20) Kozlowski, J. T.; Behrens, M.; Schlogl, R.; Davis, R. J. *ChemCatChem* **2013**, *5*, 1989.
(21) Zaki, M. I.; Hasan, M. A.; Pasupulety, L. *Langmuir* **2001**, *17*, 768.
(22) Fouad, N. E.; Thomasson, P.; Knozinger, H. *Appl. Catal., A* **2000**, *196*, 125.
(23) Zaki, M. I.; Hasan, M. A.; Al-Sagheer, F. A.; Pasupulety, L. *Langmuir* **2000**, *16*, 430.
(24) Liu, C.; Sun, J.; Smith, C.; Wang, Y. *Appl. Catal., A* **2013**, *467*, 91.
(25) Sun, J.; Zhu, K.; Gao, F.; Wang, C.; Liu, J.; Peden, C. H. F.; Wang, Y. *J. Am. Chem. Soc.* **2011**, *133*, 11096.
(26) Sun, J.; Liu, C.; Wang, Y.; Colin, S.; Kevin, M.; Padmesh, V. WO2014070354 A1, May 8th, 2014.
(27) Crisci, A. J.; Dou, H.; Prasomsri, T.; Román-Leshkov, Y. *ACS Catal.* **2014**, *4*, 4196.
(28) Jacobsen, C. J. H.; Madsen, C.; Houzvicka, J.; Schmidt, I.; Carlsson, A. *J. Am. Chem. Soc.* **2000**, *122*, 7116.
(29) Bachiller-Baeza, B.; Rodriguez-Ramos, I.; Guerrero-Ruiz, A. *Langmuir* **1998**, *14*, 3556.
(30) Li, C.; Li, M. *J. Raman Spectrosc.* **2002**, *33*, 301.
(31) Krishnankutty, N.; Vannice, M. A. *Chem. Mater.* **1995**, *7*, 754.
(32) Escalona Platero, E.; Peñarroya Mentruit, M.; Otero Areán, C.; Zecchina, A. *J. Catal.* **1996**, *162*, 268.
(33) Tanabe, K. In *Solid Acids and Bases*; Tanabe, K., Ed.; Academic Press: 1970; p 103.
(34) Rutenbeck, D.; Papp, H.; Freude, D.; Schwieger, W. *Appl. Catal., A* **2001**, *206*, 57.
(35) Yamaguchi, T.; Nakano, Y.; Tanabe, K. *Bull. Chem. Soc. Jpn.* **1978**, *51*, 2482.
(36) Idriss, H.; Barteau, M. A.; Gates, B. C.; Knozinger, H. *Adv. Catal.* **2000**, *45*, 261.
(37) Wang, H.; Schneider, W. F. *Phys. Chem. Chem. Phys.* **2010**, *12*, 6367.
(38) Takanabe, K.; Aika, K.; Seshan, K.; Lefferts, L. *Chem. Eng. J.* **2006**, *120*, 133.
(39) Cooper, P. D.; Kjaergaard, H. G.; Langford, V. S.; McKinley, A. J.; Quickenden, T. I.; Schofield, D. P. *J. Am. Chem. Soc.* **2003**, *125*, 6048.

DOI: 10.1021/jacs.5b07401
J. Am. Chem. Soc. 2016, 138, 507−517